AIAA 93-1129
GTARG - The TOPEX/POSEIDON Ground Track Maintenance Maneuver Targeting Program

Bruce E. Shapiro and
Ramachandra S. Bhat
Jet Propulsion Laboratory
California Institute of Technology
Pasadena, CA

AIAA/AHS/ASEE
Aerospace Design Conference
February 16-19, 1993 /Irvine, CA

GTARG - THE TOPEX/POSEIDON GROUND TRACK MAINTENANCE MANEUVER TARGETING PROGRAM*

Bruce E. Shapiro† ‡
Ramachandra S. Bhat‡
Jet Propulsion Laboratory, California Institute of Technology, Pasadena, Ca.

Abstract

GTARG is a computer program used to design orbit maintenance maneuvers for the TOPEX/POSEIDON satellite. These maneuvers ensure that the ground track is kept within ±1 km of an ≈9.9 day exact repeat pattern. Maneuver parameters are determined using either of two targeting strategies: *longitude targeting*, which maximizes the time between maneuvers, and *time targeting*, in which maneuvers are targeted to occur at specific intervals. The GTARG algorithm propagates non-singular (near e≈0) mean elements, taking into account anticipated error σ's in orbit determination, Δv execution, drag prediction and Δv quantization. Merson's extension of Grove's theory is used for the geopotential field. Kaula's disturbing function is used to compute the luni-solar gravitational perturbations. A satellite unique drag model is used which incorporates an approximate mean orbital Jacchia-Roberts atmosphere and a variable mean area (VMA) model. Maneuver Δv magnitudes are targeted to precisely maintain either the unbiased ground track itself, or a comfortable (3σ) error envelope about the unbiased ground track.

I. Introduction

The goal of the TOPEX/POSEIDON mission is to determine ocean surface height to an accuracy of 13 cm. (3σ) utilizing a combination of satellite altimetry data and precision orbit determination. To facilitate this mission, the satellite is maintained in a nearly circular, frozen orbit (e ≈ 0.000095, ω ≈ 90°) at an altitude of ≈1336 km. and an inclination of i ≈ 66.04°. This orbit provides an exact repeat ground track every 127 revolutions (≈ 9.9 days) and overflies two altimeter verification sites: a NASA site off the coast of Point Conception, California, and a CNES site near the islands of Lampione and Lampedusa in the Mediterranean Sea.[1,2]

The TOPEX/POSEIDON satellite was launched by Ariane on August 10, 1992 into an injection orbit which was ≈14 km. lower than the operational orbit. The operational orbit was acquired on Sep. 22, 1992, approximately 44 days after launch following six maneuvers. Subsequent maneuvers have been performed for ground track maintenance.

Mission objectives[1,3] require that at least 95% of the satellite ground tracks fall within a ±1 km. wide control band centered on a predefined reference grid and overfly the two verification sites with the same precision. Maneuvers must be spaced at least 30 days apart and occur as infrequently as possible. They are to be performed as nearly as possible to the transition between ≈ 9.9 day repeat cycles (±1 orbit), and preferably over land, to avoid disrupting altimetry data collection. Maneuver design uncertainties include Δv execution error, drag modeling unpredictability, and orbit determination accuracy.

The principal maneuver design and trajectory prediction tools available at the Jet Propulsion Laboratory (JPL) are incorporated within a family of computer programs known as the double precision trajectory system[4,5] (DPTRAJ). The trajectory generation module utilizes a predictor-corrector integrator with automatic step size control. Optimal maneuver design requires long duration orbit prediction (> 200 days) and several iterations may be required to determine a correct set of maneuver parameters. Since a DPTRAJ orbit prediction incorporating all required orbital perturbations requires ≈4.4 minutes of CPU time on the VAX-6000 computer for each day of trajectory prediction, the cost in execution time soon became prohibitive. Thus a rapid and precise analytical tool for maneuver design became necessary. GTARG was developed to meet this requirement.[6]

GTARG combines orbit prediction and targeting algorithms to design ground track maintenance

* The work described in this paper was carried out by the Jet Propulsion Laboratory, California Institute of Technology, under contract with the National Aeronautics and Space Administration.

† Member, AIAA.

‡ Member Technical Staff, Navigation Systems Section.

maneuvers. GTARG predicts the evolution of the ground track, taking into account the effects of an impulsive maneuver. Non-singular[7] mean elements[8] are propagated with dynamic models that include a high-order Earth gravity field, atmospheric drag, and luni-solar gravity. Recurrence formulae are used for the geopotential and luni-solar gravitational perturbation. Since the propagation step size is a integral multiple of the satellite's period, a polynomial fit to the mean orbital density predicted by the Jacchia-Roberts model at the TOPEX/ POSEIDON altitude is used to determine the atmospheric density.[9] A variable mean area (VMA) model[10] is used to account for drag area variation due to the nearly continuous yaw-steering of the satellite. The ground track is computed once per orbit, as the longitudinal difference at the ascending node between the actual and reference nodal longitude. The orbit is propagated either for a user specified time interval (*runout* mode) or until the ground track crosses a specified edge of the control band (*targeting* mode). Successive corrections to the Δv magnitude are made with a bisection algorithm and the orbit is again propagated until the selected control strategy is satisfied. Two control strategies are available. In *time targeting*, the ground track crosses the edge of the control band at a particular time; in *longitude targeting* the time between boundary crossings is maximized.

This paper describes the analytical models used by GTARG. A functional description of the operating modes is also given. The accuracy of the GTARG orbit propagator is assessed by calibrating with DPTRAJ using all force models. Finally, an example from TOPEX/POSEIDON mission operations illustrates the targeting process.

II. Orbit Propagation Model

The propagation algorithm[11] includes all perturbations that cause significant variations in the satellite ground track. These perturbations include Earth oblateness, luni-solar gravity, and drag. Keplerian mean elements are derived using the procedure described by Guinn.[8] The Keplerian elements serve as input to the dynamic model. Internally, the Keplerian elements are converted into a form which avoids the singularity near $e \approx 0$. These nonsingular[7] elements are a, $\xi = e\cos\omega$, $\eta = e\sin\omega$, i, Ω and $L = \omega + M$, where

a = semi-major axis,
e = eccentricity,
i = inclination,
Ω = right ascension of ascending node,
ω = argument of perigee, and
M = mean anomaly.

The mean elements are updated after each time step h to account for all perturbations. The updates are

$$a' = a + \dot{a}h \tag{1}$$
$$\xi' = \xi + \overline{\Delta\xi} + \Delta\xi_g + \Delta\xi_{ls} \tag{2}$$
$$\eta' = \eta + \overline{\Delta\eta} + \Delta\eta_g + \Delta\eta_{ls} \tag{3}$$
$$i' = i + \Delta i_g + \Delta i_{ls} \tag{4}$$
$$\Omega' = \Omega + \dot{\Omega}h + \Delta\Omega_g + \Delta\Omega_{ls} \tag{5}$$
$$L' = L + nh + \overline{\Delta L} + \Delta L_g + \Delta L_{ls} \tag{6}$$

where the primed elements are the values after the update, and the unprimed are the values before the update, and

$\dot{a}$ = rate of change in a due to drag,
n = mean motion,
$\overline{\Delta\xi}, \overline{\Delta\eta}$, and $\overline{\Delta L}$ = secular perturbation due to Earth gravity,
$\dot{\Omega}$ = secular node rate due to Earth gravity,
$\Delta i_g, \Delta\xi_g, \Delta\eta_g, \Delta L_g, \Delta\Omega_g$ = long period perturbations due to Earth gravity, and
$\Delta i_{ls}, \Delta\xi_{ls}, \Delta\eta_{ls}, \Delta L_{ls}, \Delta\Omega_{ls}$ = long period perturbations due to luni-solar gravity.

At each step all elements are initialized and perturbations are recomputed with updated elements for the next step. The Keplerian elements e, ω, and M are then obtained from

$$e = \sqrt{\xi^2 + \eta^2} \tag{7}$$
$$\omega = \tan^{-1}(\eta / \xi) \tag{8}$$
$$M = L - \omega \tag{9}$$

The eccentric anomaly is found by solving Kepler's equation[12] $M = E - e\sin E$, iteratively for E using Newton's method,

$$E_{n+1} = E_n - \frac{E_n - e\sin E_n - M}{1 - e\cos E_n} \tag{10}$$

The true anomaly v is computed by the standard transformation[12]

$$\sin v = \frac{\sqrt{1-e^2}\sin E}{1-e\cos E} \tag{11}$$

$$\cos v = \frac{\cos E - e}{1-e\cos E} \tag{12}$$

The argument of latitude u is given by $u = \omega + v$.

Each propagation step is actually performed as a sequence of shorter propagations. The advantage of this is to find the ascending node more accurately. Accurate predictions of the mean elements at the ascending node are needed since that is where the ground track is actually measured. To reduce the computation time it was decided to restrict

$$h = m\tau_n \tag{13}$$

where

h = propagation step size
m = 1, 2, 3, ..., 10, and
τ_n = nodal period.

Analysis has shown that while computation speed is linear in m, very little accuracy is lost by setting m = 10. Successive nodes are precisely located at every major step h using the method of secants on $\sin u$. The nodal crossing time is located to within 10^{-5} seconds (this corresponds to within 10 cm. in the z coordinate). Once the node has been located, the new orbital parameters are used as the starting point for the next time step h. The propagation is continued either until the desired time has elapsed or the ±1 km. control band is violated. The nodal ground track is plotted as a function of time and a summary of orbital details is printed at termination.

Geopotential Perturbations

The perturbation equations are expressed in terms of the nonsingular parameters (Appendix A). Merson's extension[13] of Grove's geopotential[14] provided the required recurrence relations. The secular effect of J_2^2 uses the explicit expressions given by Merson. The method is based upon the theory of Kozai.[15]

The recurrence formulae enable the use of zonal harmonics to any order. GTARG was implemented to include terms from J_2 through J_{29}. Due to the form of the equations, computational speed is no longer dominated by lengthy field evaluations, and hence is relatively independent of field size. The reference orbit was designed[1,2, 16] using a 17x17 subset of the GEM-T2 gravity field,[17] and later tweaked[18] with a 20x20 truncation of GEM-T3.[19] This is the minimum field size sufficient for orbit determination with the required accuracy. Thus a 20x20 truncated GEM-T3 is always used by DPTRAJ for trajectory propagation. GTARG's zonal model is also normally truncated at J_{20}, to ensure consistency with DPTRAJ, although it has the capability of using higher order terms up to J_{29}.

Luni-Solar Gravitational Perturbation

Earlier study[10] showed that luni-solar gravity is comparable in magnitude to drag at the TOPEX/POSEIDON altitude. Kaula's disturbing function[20] was used to develop expressions for the change in orbital parameters due to luni-solar gravity (Appendix B). Escobal's analytic form for the planetary ephemeris in ecliptic mean elements[12] is used to predict the positions of the sun and the moon. This analytical ephemeris was calibrated with a precision planetary ephemeris (DE118) and found to meet the accuracy requirements of GTARG.

Drag Perturbation

Earlier analysis[10] showed that for satellites in near circular orbits at altitudes > 1000 km. it is sufficient to include the effect of drag only on a. The decay rate for a satellite in a circular orbit traveling through an atmosphere fixed to a rotating planet was derived from Escobal's version[21] of Sterne's[22] result,

$$\dot{a} = -\frac{\rho A C_D \sqrt{\mu a}}{M}\left[1 - \frac{\omega_e \cos i}{n}\right]^2 \tag{14}$$

where

ρ = atmospheric density at TOPEX altitude,
A = drag area (VMA),
C_D = drag coefficient,
$\mu \approx 398600.436\ \text{km}^3/\text{sec}^2$,
M = mass of the satellite,
ω_e = earth rotation rate,
n = mean motion of the satellite,

Near-continuous yaw steering about the local nadir and solar panel pitching are utilized by the TOPEX/POSEIDON satellite to maintain the dominant 28 m^2 solar panel pointed toward the sun for power optimization. The actual pitch angle is offset from the true sun line to control the rate of battery charging. This attitude control strategy causes the true satellite drag area to continuously vary by as much as 4:1 during a single orbit period.[10]

This continuously variable area (CVA) is a rapid periodic function of orbit angle whose extrema are a slowly varying function of β', the angle between the orbit plane and the earth-sun line. The maximum CVA amplitude occurs when $\beta'=0$, while the minimum drag area coincides with the local maxima of β'. The period of β' variation is ≈56 days. The use of a CVA model for orbit determination and prediction is computationally intense. Instead, required accuracies are achieved with an approximate variable mean area (VMA) model, which defines the mean area per orbit as a tabular function of β'. The VMA model performance was calibrated using the CVA.

Atmospheric density is computed using a simple polynomial fit of the average orbital log density as a function of the modified exospheric temperature $\hat{T}_\infty$,

$$\hat{T}_\infty = 379^\circ + 3.24^\circ \overline{F_{10.7}} + 1.3^\circ \left[F_{10.7} - \overline{F_{10.7}}\right] + 28^\circ K_p + 0.03^\circ e^{K_p} \quad (15)$$

where

$F_{10.7}$ = uncorrected daily 10.7 cm. solar flux,
$\overline{F_{10.7}}$ = 81-day centered average of the 10.7 cm solar flux, and
K_p = daily planetary geomagnetic index.

The polynomial was developed[9] by a least squares fit to the Jacchia-Roberts model[22] using solar and geomagnetic data over the entire solar cycle 21.

Maneuver Modeling

GTARG predicts the ground track evolution following an impulsive maneuver, measured with respect to the reference track. The maneuver is defined in terms of magnitude (ΔV) and direction, represented by the angles α and δ in the local-horizontal/local-vertical (LHLV) coordinate frame. The LHLV frame moves with the satellite. The z-axis of the LHLV frame is defined by the satellite radius vector, the y-axis by the orbit normal, and the x-axis completes a right handed coordinate system. In this frame α is the angle between the x-axis and the projection of the maneuver vector on the x-y plane, and δ is the angle between the x-y plane and the maneuver vector. For most orbit maintenance maneuvers $\alpha = \delta = 0$. The maneuver is applied by transforming the pre-maneuver elements into a nearly-inertial Earth centered Cartesian reference frame (Escobal's PQW frame[19]), and then into the LHLV frame. The components of ΔV are then added directly to the velocity vector. The post-maneuver elements are computed by transforming the LHLV state back into Keplerian elements.

III. Calibration With Numerical Integrator

Since maintenance maneuvers are scheduled as infrequently as possible, they should be targeted with maximum accuracy. For scheduling purposes, the date of a maneuver is preferentially determined at least one month in advance, and this date must coincide to the transition between ground track repeat cycles. Accurate targeting is ensured by calibrating GTARG with DPTRAJ.

The targeting algorithm is described below in detail (sec. VI). Procedurally, GTARG is used as follows. The maneuver magnitude is first determined with GTARG and then verified with DPTRAJ. The maneuver is implemented in DPTRAJ by applying a finite burn whose magnitude equals the GTARG impulsive ΔV, and whose centroid time coincides with the GTARG burn time. The resulting post-maneuver mean elements and ground track histories are then examined. This process is iterated until satisfactory results are obtained in DPTRAJ with all force models enabled.

This process will require multiple iterations if the first ΔV estimate is poor; the entire procedure quickly becomes prohibitively CPU-expensive. If GTARG is sufficiently precise at predicting the ground track, however, the number of GTARG-DPTRAJ iterations can be reduced to one. The DPTRAJ run then becomes one of maneuver validation rather than maneuver targeting, and the entire targeting process becomes far more manageable.

The CPU time required for a GTARG run, including the error model, Earth gravity to J_{20}, drag, and luni-solar gravity, is $\approx 0.14/m$ minutes for each day of propagation, where m is the GTARG propagation step size in orbits. This result is relatively independent of the size of the gravity field, decreasing by only ≈20% when the field is truncated at J_2. Comparing this with the value quoted above (sec. I) for DPTRAJ (4.4 minutes/day) gives

$$\frac{Speed\ of\ GTARG}{Speed\ of\ DPTRAJ} \approx 94m \approx 940 \quad (\text{for } m = 10)$$

or an increase in processing speed by approximately three orders of magnitude when GTARG is used in place of DPTRAJ.

The mean orbital parameters which are input to GTARG are derived from the operational orbit ephemeris (OOE). The OOE, which is produced by DPTRAJ, is based upon a numerical integration of the satellite state vector which includes all relevant perturbing forces (oblate Earth, luni-solar gravity, atmospheric drag, solar radiation pressure, solid earth tides, polar motion, precession, and nutation). It is used for mission planning, command scheduling, TDRS and DSN acquisition, satellite clock calibration, star tracker initialization and satellite pointing control via on-board ephemeris loads, science data processing and instrument initialization, and verification of the ground track repeatability. Predicted post-maneuver OOE files are generated prior to all maneuvers as well as on a weekly basis for satellite ephemeris loads. The method given by Guinn[8] is used for the conversion between the osculating state in the OOE and the mean elements used by GTARG.

Compatibility between the DPTRAJ and GTARG mean elements is ensured as follows. A reference orbit can be defined by turning off all perturbations except for Earth gravity and tweaking the elements until the ground track repeats after 127 revolutions. This procedure can be performed with either DPTRAJ or GTARG. Let $\hat{M}_i^{DPTRAJ}$ be the reference mean elements derived with DPTRAJ, and $\hat{M}_i^{GTARG}$ be a similar set of reference elements derived with GTARG. In general, $\hat{M}_i^{GTARG} \neq \hat{M}_i^{DPTRAJ}$ because of propagation and other modeling differences. The mean elements M_i^{GTARG} used for propagation by GTARG are then obtained from the mean elements derived from the OOE, M_i^{DPTRAJ}, as

$$M_i^{GTARG} = M_i^{DPTRAJ} + \hat{M}_i^{GTARG} - \hat{M}_i^{DPTRAJ} \qquad (16)$$

In particular, DPTRAJ models tesseral field harmonics, time transformations (e.g., UT1-UTC), solid earth tides, precession, nutation and polar motion, none of which are modeled by GTARG. DPTRAJ is updated whenever new timing and polar motion data become available, usually weekly. These changes primarily affect the semi-major axis a and right ascension of node Ω because the TOPEX/POSEIDON satellite is in a frozen orbit. The calibration procedure defined by eq. (16) is repeated whenever new data is added to the system.

After each calibration, 30-day trajectories are generated with both DPTRAJ and GTARG and compared to verify GTARG's accuracy. Fig. 1 shows a typical comparison of the equatorial crossing longitudes using data following orbit maintenance maneuver 1 (OMM1). OMM1 took place on September 12, 1992 at 23:13:30 UTC. DPTRAJ used a 20x20 truncation of the GEM-T3 gravity field, while GTRAG used a 20th order zonal field to produce these results. Although a complete statistical analysis encompassing all parametric variations has not been performed, the longitudinal difference in nodal crossings between DPTRAJ and GTARG is less than ≈75 meters after 30 days for every case we have examined. While the shape (and even the sign of the difference) will vary from fig. 1 for different starting epochs due to changes in the luni-solar geometry and differences in drag, the essential result will not.

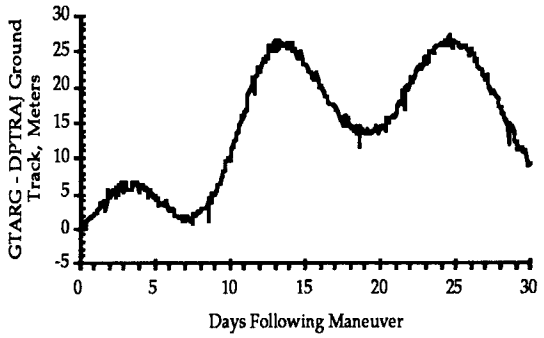

Fig. 1. Comparison between DPTRAJ and GTARG following Orbit Maintenance Maneuver 1.

IV. Complexity of GTARG

GTARG has been shown to be both sufficiently complex and sufficiently accurate to meet the requirements placed upon it. But might a simpler method have been sufficient? This can be answered be examining each of the dynamic models incorporated within GTARG: a zonal Earth gravity field, drag, and luni-solar gravity. The necessity of including drag and luni-solar gravity have been demonstrated elsewhere.[10] Fig. 2 shows the error in the ground track calculation predicted by GTARG as a function of Earth gravity field size starting from an epoch of Nov. 3, 1992. The satellite ground track

remained well within the control band for the period shown. The error is calculated by assuming that a DPTRAJ run with a 20x20 gravity field and all perturbations enabled represented the truth. While the actual values shown will change with variations in solar activity (hence drag) and luni-solar geometry, the essential characteristic will not. If J_M is the highest order zonal term used, then the algorithm represents a converged trajectory if the magnitude of the error never exceeds the fraction of the error budget which is allocated to propagation errors for all $m > M$. Fig. 2 shows that a zonal field of at least 12th order is required to obtain an accuracy of 50 meters after 30 days. Thus a simpler technique, such as a two body propagation with J2, would not be sufficient. Furthermore, all precision parameters are derived via a 20x20 geopotential; for maximum compatibility between the mean and osculating element sets, one would expect optimal convergence at J_{20}. Since the algorithmic complexity is only weakly dependent on the field size, nothing is lost by using a larger field in GTARG. Hence GTARG has the minimum amount of complexity required.

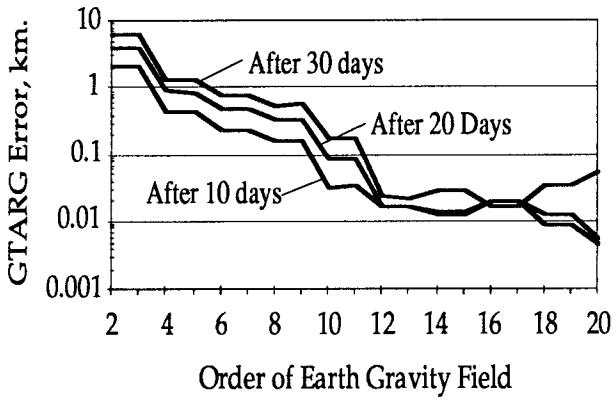

Fig. 2. Error in ground track calculation by GTARG. The "truth" is given by DPTRAJ.

V. Error Models

Eastern and western error envelopes on the ground track are calculated for the ground track along with the unbiased track. These are illustrated in fig. 3. The error envelope defines the most eastward and most westward ground tracks which can reasonably be expected with a specified degree of confidence.

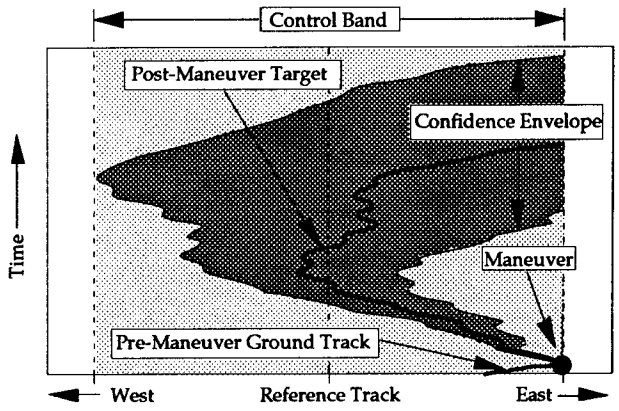

Fig. 3. Ground track confidence envelope.

The longitudinal width of the envelope is derived from anticipated maneuver execution, orbit determination (OD), and drag prediction errors. The drag modeling error is dominated by uncertainties in solar activity prediction. Maneuver execution errors are categorized into fixed, proportional, and pointing errors. An error in maneuver execution translates into a ground track error as

$$\delta(\Delta\lambda)_{\Delta V} \approx \frac{\partial(\Delta\lambda)}{\partial V}\delta(\Delta V) \approx \frac{-3\omega_e t}{V}\delta(\Delta V) \qquad (17)$$

where

$\Delta\lambda$ = ground track longitudinal difference from reference measured at the ascending node,

$\delta(\Delta\lambda)_{\Delta V}$ = 1σ error in $\Delta\lambda$ due to $\delta(\Delta V)$,

$\delta(\Delta V)$ = 1σ error in maneuver implementation,

ω_e = earth rotation rate,

t = time following maneuver, and

V = satellite orbital velocity.

The orbit determination error is reflected primarily as an error in the semi-major axis; the corresponding ground track error becomes

$$\delta(\Delta\lambda)_{OD} \approx \frac{\partial(\Delta\lambda)}{\partial a}(\Delta a)_{OD} \approx \frac{3\omega_e t}{2a}(\Delta a)_{OD} \qquad (18)$$

where

$\delta(\Delta\lambda)_{OD}$ = 1σ error $\Delta\lambda$ due to OD errors, and

$(\Delta a)_{OD}$ = 1σ OD error in a.

Anticipated error σ's in the solar and geomagnetic indices $F_{10.7}$, $\overline{F_{10.7}}$, and K_p are used to generate high-density and low-density trajectories; the

resulting differences in the ground track with the error-free trajectory are used to calculate the drag error $\delta(\Delta\lambda)_{DRAG}$.

The three types of errors are propagated, converted into ground track units, and then combined to predict a total root-sum-square (RSS) error envelope in the ground track. The terms in the sum are weighted to produce the desired level of confidence

$$\left[\delta(\Delta\lambda)\right]^2 = \kappa_{OD}^2\left[\delta(\Delta\lambda)_{OD}\right]^2 + \kappa_{\Delta V}^2\left[\delta(\Delta\lambda)_{\Delta V}\right]^2 + \kappa_{Drag}^2\left[\delta(\Delta\lambda)_{Drag}\right]^2 \quad (19)$$

where

κ_{OD}, $\kappa_{\Delta V}$, κ_{Drag} = scale factors for OD, maneuver execution, and drag estimation,

$\delta(\Delta\lambda)$ = total error budget (half-with of the confidence envelope).

The nominal TOPEX/POSEIDON confidence level is 95%. Assuming that the errors are distributed normally, this corresponds to the 1.96σ ($\kappa = 1.96$) error level.

VI. Targeting Algorithm

Two classes of targeting strategies are implemented in GTARG: *longitude targeting* and *time targeting*. These are illustrated in fig. 4.

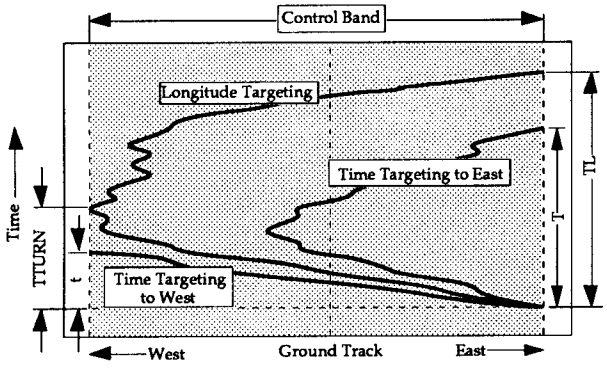

Fig. 4. Longitude and time targeting strategies. The control band is shaded.

Longitude targeting utilizes the full control band to maximize the time between maneuvers. Applying a ΔV at the eastern edge of the band, the semi-major axis is increased. The resulting higher nodal period causes the ground track to drift westward. Drag continuously reduces the nodal period until the ground track becomes just tangent to the western boundary; the ground track then reverses eastward as the period continues to decrease. Eventually the ground track returns to the eastern boundary after a time *TL*. (shown in fig. 4).

Alternatively, in *time targeting*, the time between maneuvers is selected first. A smaller ΔV, which will allow the ground track to return to the eastern boundary sooner than *TL* (*T* in fig. 4), is utilized for *time targeting to the eastern boundary*. Similarly, in *time targeting to the western boundary*, a larger ΔV is used, causing the ground track to cross the western boundary some time *t* prior to the longitude targeting turn-around time *TTURN*. GTARG implements these three targeting schemes along with a simple *runout* mode in which the ground track profile is predicted but no maneuver targeting is performed.

Targeting involves determination of the approximate ΔV magnitude for the selected targeting mode. GTARG makes as its first guess a constant-drag approximation, ignoring the earth oblateness and lunar and solar gravity perturbations. Starting with equation (4) of reference (10), for longitude targeting,

$$\Delta V_0 = \sqrt{(\Delta\lambda_0 - \Delta\lambda_{West})\frac{\rho C_D A}{3m\omega_e}V^3} \quad (20)$$

where $\Delta\lambda_0$ is the initial ground track and $\Delta\lambda_{West}$ is the ground track of the western boundary. For time targeting to the eastern boundary after a time *T*,

$$\Delta V_0 = \frac{\rho A C_D V^2 T}{4m} - \frac{(\Delta\lambda_{East} - \Delta\lambda_0)V}{3T\omega_e} \quad (21)$$

The trajectory is then successively propagated and the ΔV is modified, until a satisfactory value of ΔV, which produces the desired ground track evolution, is found. For *longitude targeting*, successful targeting means that the westernmost ground track of the western confidence envelope just reaches (within a user-supplied tolerance) but does not cross the western edge of the control band (as in fig. 3). For *time targeting*, the desired confidence envelope will reach the desired edge of the control within a user-specified tolerance of the targeted time. The second iteration will either increase or decrease ΔV, depending upon whether the targeted ground track is overshot or undershot. Subsequent iterations for

ΔV are found by linear interpolation on the maximum westward ground track (for *longitude targeting)* or time of leaving the control band (for *time targeting*). The algorithm may terminate earlier if successive ΔV guesses are smaller than the allowed command quantization level.

VII. Targeting Example

The first TOPEX/POSEIDON ground track maintenance maneuver was implemented on October 12, 1992. The pre-maneuver state was approximately 10 meters beneath the repeat orbit; the targeted post maneuver orbit was approximately 21 meters higher than the pre-maneuver state (targeted $\Delta V \approx 9.18$ mm/sec). The maneuver details are shown in fig. 5. Inputs to the error model included fixed and proportional ΔV errors of $\sigma_{fixed} = .004433$ mm/sec and $\sigma_{proportional} = 1.67\%$, and orbit determination errors of $\sigma_{\Delta a} = 33$ cm. The errors were assumed to be normally distributed and the 95% confidence limits set to 1.96σ. The algorithm for the prediction of solar flux and computation of the 81-day centered average described in reference (9) was used to produce the solar and geomagnetic data profile, based upon the most recent 27-day Space Environment Services Center (SESC) outlook. A constant value of K_P=2.6, the average of the most recent 27-day available at the time of the targeting process, was used after 27 days. $F_{10.7}$ was predicted by repeated the 27-day outlook as required; the 81-day centered average, $\overline{F_{10.7}}$, was built from these predictions. A statistical analysis of the accuracy of this method for the first 9 months of 1992 was used to generate the solar and geomagnetic error σ's.

VIII. Summary

GTARG is a rapid and accurate analytical tool which was developed to generate strategies for ground track maintenance maneuvers. It incorporates the effects of error sources and the minimal set of dynamical models needed for ground track accuracy. These models include central body gravity with zonal perturbations to at least the J_{20}, luni-solar gravity, and drag. The mean element propagation scheme and simplified drag model allow for an increase in the throughput speed of a single run by nearly three orders of magnitude. At the same time, accuracy is not severely impacted by the simplification of models when it is measured in terms of equatorial crossing at ascending node. Since such a measurement is sufficient for maneuver targeting, multiple numerical integration targeting iterations can be replaced by a single GTARG targeting run followed by a single DPTRAJ numerical orbit integration for precise design verification. A timely calibration scheme has been developed to ensure the compatibility between GTARG and DPTRAJ mean elements.

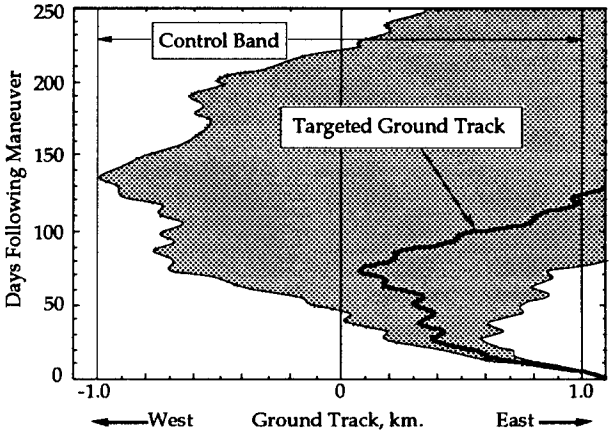

Fig. 5. Targeted and 95% Confidence band (shaded) for Orbit Maintenance Maneuver #1.

Both longitude and time targeting strategies have been demonstrated with an example from the TOPEX/POSEIDON mission using errors in orbit determination, thrust execution and drag prediction. These error estimates are used to predict the ground track with a 95% certainty. The versatility of GTARG stems from both its accuracy and its speed, which allow for exploration of the parametric dependence of ground track upon data variations at a fraction of the cost of orbital integration while still maintaining a high degree of confidence in the ability to correctly predict the ground track.

Acknowledgment

P. E. Cannell implemented the initial versions of GTARG. We thank R. B. Frauenholz for his valuable guidance and support throughout the development of the software.

Appendix A. Earth Gravity Model

Merson's extension[13] of Groves' theory[14] is implemented to 29th order in the geopotential field. Given the orbital elements the following items are calculated:

$$n_0 = \sqrt{\frac{\mu}{a^3}} \tag{A-1}$$

$$n = n_0\left[1+\tfrac{3}{2}J_2(R_e/p)^2\sqrt{1-e^2}\left(1-\tfrac{3}{2}\sin^2 i_0\right)\right] \tag{A-2}$$

$$p = a(1-e^2) \tag{A-3}$$

where R_e is the equatorial radius of the earth. Let l and k be indices where $l \geq 2$ and $0 \leq k \leq l$. Define the functions

$$v = \tfrac{1}{2}(l-k). \tag{A-4}$$

$$u_k = \begin{cases} 1, & k = 0 \\ 2, & k \neq 0 \end{cases} \tag{A-5}$$

$$T_l^k(0) = \begin{cases} 0, & (l-k)\ odd \\ \dfrac{(-1)^v(l+k)!}{2^l v!(l-v)!}, & (l-k)\ even \end{cases} \tag{A-6}$$

$$\gamma_l^k = -\frac{u_k(l-1)!T_l^k(0)n(R_e/p)^l}{2^{2k}k!k!(l-k-1)!} \tag{A-7}$$

$$\alpha_l^k = \frac{(l+k+1)(l-k)}{2(k+1)} \tag{A-8}$$

$$\beta_l^k = \alpha_{l-1}^k. \tag{A-9}$$

The inclination function is defined for $l \geq 2$ and $k \geq 1$ as

$$A_k^k = 1 \tag{A-10}$$

$$A_{k+1}^k = \cos i \tag{A-11}$$

$$A_l^{k-1} = A_l^k \cos i - \frac{\alpha_l^k \sin^2 i}{2k} A_l^{k+1} \tag{A-12}$$

The eccentricity functions are defined for $l \geq 2$ and $1 \leq k \leq l$,

$$B_k^k = 0 \tag{A-13}$$

$$B_{k+1}^k = 1 \tag{A-14}$$

$$B_l^{k+1} = B_l^k + \frac{\beta_l^k e^2}{2k} B_l^{k+1} \tag{A-15}$$

The secular perturbations due to the zonal harmonics thus are

$$\dot{\Omega}_{zonal} = -\sum_{l=2}^{l_{max}} J_l \gamma_l^0 B_l^0 A_l^1 \tag{A-16}$$

$$\dot{\omega}_{zonal} = \sum_{l=2}^{l_{max}} J_l\gamma_l^0\left[\alpha_l^0 B_l^0 A_l^1 \cos i + A_l^0(lB_l^0 + \beta_l^0 B_l^1)\right] \tag{A-17}$$

$$n_{zonal} = \sum_{l=3}^{l_{max}} qJ_l\gamma_l^0 A_l^0[(l-1)B_l^0 - B_l^1\beta_l^0] \tag{A-18}$$

where $q = 1\text{-}e^2$. The secular perturbations due to J_2^2 are

$$\dot{\Omega}_2 = \tfrac{3}{32}nJ_2^2(R_e/p)^4 \times \left[\left(4+12\sqrt{1-e^2}-9e^2\right)\cos i - \left(40+36\sqrt{1-e^2}-5e^2\right)\cos^3 i\right] \tag{A-19}$$

$$\dot{\omega}_2 = -\tfrac{3}{128}nJ_2^2\left(\frac{R_e}{p}\right)^4\left[10-24\sqrt{1-e^2}+25e^2+\left(36+192\sqrt{1-e^2}-126e^2\right)\cos^2 i - \left(430+360\sqrt{1-e^2}-45e^2\right)\cos^4 i\right] \tag{A-20}$$

$$n_2 = \tfrac{3}{128}nJ_2^2\left(\frac{R_e}{p}\right)^4\sqrt{1-e^2}\left[16\sqrt{1-e^2}-25e^2-\left(60+96\sqrt{1-e^2}-90e^2\right)\cos^2 i + 10+\left(130+144\sqrt{1-e^2}-25e^2\right)\cos^4 i\right] \tag{A-21}$$

Thus the secular rates become

$$\dot{\Omega}_s = \dot{\Omega}_{zonal} + \dot{\Omega}_2 \tag{A-22}$$

$$\dot{\omega}_s = \dot{\omega}_{zonal} + \dot{\omega}_2 \tag{A-23}$$

$$n_s = n_{zonal} + n_2 \tag{A-24}$$

$$\dot{L}_s = n_s + \dot{\omega}_s \tag{A-25}$$

and the updates to the secular perturbations are

$$\overline{\Delta\xi} = \xi_0(\cos\dot{\omega}_s h - 1) - \eta_0\sin(\dot{\omega}_s h) \tag{A-26}$$

$$\overline{\Delta\eta} = \eta_0(\cos\dot{\omega}_s h - 1) + \xi_0\sin(\dot{\omega}_s h) \tag{A-27}$$

$$\overline{\Delta L} = \dot{L}_s h \tag{A-28}$$

The long periodic perturbations due to gravity can also be broken up into two parts: the J_n contributions and the J_2^2 contributions.

$$\Delta a = 0 \tag{A-29}$$
$$\Delta\xi_g = \Delta\xi_1 + \Delta\xi_2 \tag{A-30}$$
$$\Delta\eta_g = \Delta\eta_1 + \Delta\eta_2 \tag{A-31}$$
$$\Delta i_g = \Delta i_1 + \Delta i_2 \tag{A-32}$$
$$\Delta\Omega_g = \Delta\Omega_1 + \Delta\Omega_2 \tag{A-33}$$
$$\Delta L_g = \Delta L_1 + \Delta L_2 \tag{A-34}$$

where a subscript of 1 indicates the zonal contributions and a subscript of 2 indicates a J_2^2 effect. To obtain the long term perturbations due to the zonal harmonics, first define the following coefficients on the range $l \geq 3, 1 \leq k \leq l-2$.

$$a_{lk} = J_l\,\gamma_l^k\,(e\sin i)^k A_l^k B_l^k \tag{A-35}$$
$$a'_{lk} = kJ_l\,\gamma_l^k\,(e\sin i)^{k-1} A_l^k B_l^k \tag{A-36}$$
$$b_{lk} = lJ_l\,\gamma_l^k\,(e\sin i)^k A_l^k B_l^k \tag{A-37}$$
$$c_{lk} = J_l\,\gamma_l^k\,(e\sin i)^k A_l^{k+1} B_l^k \alpha_l^k \tag{A-38}$$
$$d_{lk} = J_l\,\gamma_l^k\,(e\sin i)^k A_l^k B_l^{k+1} \beta_l^k \tag{A-39}$$
$$\begin{aligned} C_k &= \int_0^h \cos k\left(\omega - \tfrac{\pi}{2}\right) dt \\ &\approx h\left[F_1 \cos k\left(\omega - \tfrac{\pi}{2}\right) - k\dot{\omega}_s h F_2 \sin k\left(\omega - \tfrac{\pi}{2}\right)\right] \end{aligned} \tag{A-40}$$
$$\begin{aligned} S_k &= \int_0^h \sin k\left(\omega - \tfrac{\pi}{2}\right) dt \\ &\approx h\left[k\dot{\omega}_s h F_2 \cos k\left(\omega - \tfrac{\pi}{2}\right) + F_1 \sin k\left(\omega - \tfrac{\pi}{2}\right)\right] \end{aligned} \tag{A-41}$$

where the expansions

$$F_1 = 1 - \frac{x^2}{3!} + \frac{x^4}{5!} - \frac{x^6}{7!} + \cdots \tag{A-42}$$
$$F_2 = \frac{1}{2} - \frac{x^2}{24} + \frac{x^4}{720} + \cdots \tag{A-43}$$

have been used, with $x = k\dot{\omega}_s h$. Then

$$\begin{aligned} \Delta\xi_1 = {} & q^2 \sin i \cos\omega_0 \sum_{l=3}^{l_{max}} \sum_{k=1}^{l-2} a'_{lk} S_k - \\ & \left(\sin^2 i - e^2 \cos^2 i\right) \frac{\sin\omega_0}{\sin i} \sum_{l=3}^{l_{max}} \sum_{k=1}^{l-2} a'_{lk} C_k - \\ & \eta_0 \sum_{l=3}^{l_{max}} \sum_{k=1}^{l-2} (b_{lk} + d_{lk} + c_{lk}\cos i) C_k \end{aligned} \tag{A-44}$$

$$\begin{aligned} \Delta\eta_1 = {} & q^2 \sin i \sin\omega_0 \sum_{l=3}^{l_{max}} \sum_{k=1}^{l-2} a'_{lk} S_k - \\ & \left(\sin^2 i - e^2 \cos^2 i\right) \frac{\cos\omega_0}{\sin i} \sum_{l=3}^{l_{max}} \sum_{k=1}^{l-2} a'_{lk} C_k + \\ & \xi_0 \sum_{l=3}^{l_{max}} \sum_{k=1}^{l-2} (bl_k + d_{lk} + c_{lk}\cos i) C_k \end{aligned} \tag{A-45}$$

$$\Delta i_1 = -e\cos i \sum_{l=3}^{l_{max}} \sum_{k=1}^{l-2} a'_{lk} S_k \tag{A-46}$$

$$\Delta\Omega_1 = \sum_{l=3}^{l_{max}} \sum_{k=1}^{l-2} \left[e \frac{\cos i}{\sin i} a'_{lk} - c_{lk} \right] C_k \tag{A-47}$$

$$\begin{aligned} \Delta L_1 = \sum_{l=3}^{l_{max}} \sum_{k=1}^{l-2} \Big[& (1+q) b_{lk} - e \frac{\cos^2 i}{\sin i} a'_{lk} + \\ & c_{lk}\cos i - a_{lk} \Big] C_k \end{aligned} \tag{A-48}$$

The J_2^2 contribution to the long period perturbations is

$$\begin{aligned} \Delta\xi_2 = {} & -\tfrac{3}{64} n J_2^2 (R_e/p)^4 \times \\ & \Big\{ 2\xi\left(1-e^2\right)\left(1 - 16\cos^2 i + 15\cos^4 i\right) S_2 - \\ & \eta\Big[\left(2+5e^2\right) - \left(32 + 112e^2\right)\cos^2 i + \\ & \left(30 + 135e^2\right)\cos^4 i \Big] C_2 \Big\} \end{aligned} \tag{A-49}$$

$$\begin{aligned} \Delta\eta_2 = {} & -\tfrac{3}{64} n J_2^2 (R_e/p)^4 \times \\ & \Big\{ 2\eta\left(1-e^2\right)\left(1 - 16\cos^2 i + 15\cos^4 i\right) S_2 + \\ & \xi\Big[\left(2+5e^2\right) - \left(32 + 112e^2\right)\cos^2 i + \\ & \left(30 + 135e^2\right)\cos^4 i \Big] C_2 \Big\} \end{aligned} \tag{A-50}$$

$$\Delta i_2 = -\tfrac{21}{16} n J_2^2 \left(\frac{R_e}{p}\right)^4 e^2 \sin i \cos i \left(1 - \tfrac{15}{14}\sin^2 i\right) S_2 \tag{A-51}$$

$$\Delta\Omega_2 = -\tfrac{3}{32} n J_2^2 \left(\frac{R_e}{p}\right)^4 e^2 \cos i \left(16 - 30\cos^2 i\right) S_2 \tag{A-52}$$

$$\begin{aligned} \Delta L_2 = {} & -\tfrac{3}{64} n J_2^2 \left(\frac{R_e}{p}\right)^4 C_2 \Big[\sqrt{1-e^2}\left(5e^2 - 2\right) \times \\ & \left(1 - 16\cos^2 i + 15\cos^4 i\right) + \\ & \left(2 + 5e^2\right) - \left(32 + 112e^2\right)\cos^2 i + \\ & \left(30 + 135e^2\right)\cos^4 i \Big] \end{aligned} \tag{A-53}$$

Appendix B. Lunar-Solar Gravitational Perturbation

Kaula's disturbing function[20] is used to compute the lunar-solar gravitational potential

$$R = \sum_{l=2}^{l_{max}} \mu_J \frac{a^l}{a_J^{l+1}} \sum_{m=0}^{l} d \frac{(l-m)!}{(l+m)!} \times \sum_{p=0}^{l} \sum_{h=0}^{l} \sum_{j=-1}^{1} F_{lmp}(i) F_{lmh}(i_J) \times H_{lp0}(e) G_{lhj}(e_J) \cos Y \tag{B-1}$$

where $\{a_J, e_J, i_J, \Omega_J, \omega_J, M_J\}$ are the elements of the sun or the moon ($J = sun$ or $J = moon$), $F_{lmp}(i)$ is the inclination function of the satellite, $F_{lmh}(i_J)$ is the inclination function of the sun or the moon, $H_{lp0}(e)$ is the eccentricity function of the satellite, $G_{lhj}(e_J)$ is the eccentricity function of the sun or the moon,

$$d = \begin{cases} 1, & m = 0 \\ 2, & m \neq 0 \end{cases} \tag{B-2}$$

and

$$Y = m(\Omega - \Omega_J) - (l-2h)\omega_J - (l-2h+j)M_J \tag{B-3}$$

The perturbations are then expressed as

$$\Delta a_{ls} = 0 \tag{B-4}$$

$$\Delta \xi_{ls} = \frac{\eta}{na^2} \sum_{l=2}^{l_{max}} \mu_J \frac{a^l}{a_J^{l+1}} \sum_{m=0}^{l} d \frac{(l-m)!}{(l+m)!} \sum_{p=0}^{l} \sum_{h=0}^{l} \sum_{j=-1}^{1} F_{lmh}(i_J) G_{lhj}(e_J) \times \left[\frac{\cos i}{\sin i \sqrt{1-e^2}} \frac{d}{di} F_{lmp}(i) H_{lp0}(e) - \frac{\sqrt{1-e^2}}{e} F_{lmp}(i) \frac{d}{de} H_{lp0}(e) \right]_0^h \int \cos Y dt \tag{B-5}$$

$$\Delta \eta_{ls} = \frac{\xi}{na^2} \sum_{l=2}^{l_{max}} \mu_J \frac{a^l}{a_J^{l+1}} \sum_{m=0}^{l} d \frac{(l-m)!}{(l+m)!} \times \sum_{p=0}^{l} \sum_{h=0}^{l} \sum_{j=-1}^{1} F_{lmh}(i_J) G_{lhj}(e_J) \times \left[\frac{\sqrt{1-e^2}}{e} F_{lmp}(i) \frac{d}{de} H_{lp0}(e) - \frac{\cos i}{\sin i \sqrt{1-e^2}} \frac{d}{di} F_{lmp}(i) H_{lp0}(e) \right]_0^h \int \cos Y dt \tag{B-6}$$

$$\Delta i_{ls} = \frac{1/na^2}{\sin i \sqrt{1-e^2}} \sum_{l=2}^{l_{max}} \mu_J \frac{a^l}{a_J^{l+1}} \sum_{m=0}^{l} d \frac{(l-m)!}{(l+m)!} \times \sum_{p=0}^{l} \sum_{h=0}^{l} \sum_{j=-1}^{1} F_{lmp}(i) F_{lmh}(i_J) \times H_{lp0}(e) G_{lhj}(e_J) m \int_0^h \sin Y dt \tag{B-7}$$

$$\Delta \Omega_{ls} = \frac{1/na^2}{\sin i \sqrt{1-e^2}} \sum_{l=2}^{l_{max}} \mu_J \frac{a^l}{a_J^{l+1}} \sum_{m=0}^{l} d \frac{(l-m)!}{(l+m)!} \times \sum_{p=0}^{l} \sum_{h=0}^{l} \sum_{j=-1}^{1} \frac{d}{di} F_{lmp}(i) F_{lmh}(i_J) \times H_{lp0}(e) G_{lhj}(e_J) \int_0^h \cos Y dt \tag{B-8}$$

$$\Delta L_{ls} = -\frac{1}{na^2} \sum_{l=2}^{l_{max}} \mu_J \frac{a^l}{a_J^{l+1}} \sum_{m=0}^{l} d \frac{(l-m)!}{(l+m)!} \times \sum_{p=0}^{l} \sum_{h=0}^{l} \sum_{j=-1}^{1} F_{lmh}(i_J) H_{lp0}(e) G_{lhj}(e_J) \times \left(2l F_{lmp}(i) + \frac{\cos i}{\sqrt{1-e^2} \sin i} \frac{d}{di} F_{lmp}(i) \right) \times \int_0^h \cos Y dt \tag{B-9}$$

To solve the integrals, substitute $x = \dot{Y}t$, where

$$\dot{Y} = m\dot{\Omega} - (l-2h+j)n_J. \tag{B-10}$$

Then

$$\int_0^h \sin Y dt = h\left[xF_2 \cos Y_0 + F_1 \sin Y_0 \right] \tag{B-11}$$

$$\int_0^h \cos Y dt = h\left[-xF_2 \sin Y_0 + F_1 \cos Y_0 \right] \tag{B-12}$$

Assigning $l_{\max} = 2$ then $m = 0,1,2$, $p = 1$, $j = -1,0,1$, and $h = 0,1,2$. With this the eccentricity and inclination functions may be calculated. The general form of $H_{lp0}(e)$ is given by

$$H_{lp0}(e) = 1 + \tfrac{1}{4}(l - 3l^2 + 16lp - 16p^2)e^2 \qquad \text{(B-13)}$$

hence

$$H_{200} = 1 - \tfrac{5}{2}e^2 \qquad \text{(B-14)}$$

$$H_{210} = 1 + \tfrac{3}{2}e^2 \qquad \text{(B-15)}$$

$$H_{220} = 1 - \tfrac{5}{2}e^2 \qquad \text{(B-16)}$$

$$\frac{\partial}{\partial e}H_{200} = -5e \qquad \text{(B-17)}$$

$$\frac{\partial}{\partial e}H_{210} = 3e \qquad \text{(B-18)}$$

$$\frac{\partial}{\partial e}H_{220} = -5e \qquad \text{(B-19)}$$

Similarly

$$G_{20-1} = -\tfrac{1}{2}e_J - \tfrac{1}{16}e_J^3 \qquad \text{(B-20)}$$

$$G_{200} = 1 - \tfrac{5}{2}e_J^2 + \tfrac{13}{16}e_J^4 \qquad \text{(B-21)}$$

$$G_{201} = \tfrac{7}{2}e_J - \tfrac{123}{16}e_J^3 \qquad \text{(B-22)}$$

$$G_{21-1} = \tfrac{3}{2}e_J + \tfrac{27}{16}e_J^3 \qquad \text{(B-23)}$$

$$G_{210} = \left(1 - e_J^2\right)^{-3/2} \qquad \text{(B-24)}$$

$$G_{211} = G_{21-1} \qquad \text{(B-25)}$$

$$G_{22-1} = G_{201} \qquad \text{(B-26)}$$

$$G_{220} = G_{200} \qquad \text{(B-27)}$$

$$G_{221} = G_{20-1} \qquad \text{(B-28)}$$

and the inclination functions F and $\partial F/\partial i$ become

$$F_{200} = -\tfrac{3}{8}\sin^2 i \qquad \text{(B-29)}$$

$$F_{201} = \tfrac{3}{4}\sin^2 i - \tfrac{1}{2} \qquad \text{(B-30)}$$

$$F_{202} = F_{200} \qquad \text{(B-31)}$$

$$F_{210} = \tfrac{3}{4}\sin i(1 + \cos i) \qquad \text{(B-32)}$$

$$F_{211} = -\tfrac{3}{2}\sin i\cos i \qquad \text{(B-33)}$$

$$F_{212} = -\tfrac{3}{4}\sin i(1 - \cos i) \qquad \text{(B-34)}$$

$$F_{220} = \tfrac{3}{4}(1 + \cos i)^2 \qquad \text{(B-35)}$$

$$F_{221} = \tfrac{3}{2}\sin^2 i \qquad \text{(B-36)}$$

$$F_{222} = \tfrac{3}{4}(1 - \cos i)^2 \qquad \text{(B-37)}$$

and

$$\frac{\partial}{\partial i}F_{200} = -\tfrac{3}{4}\sin i\cos i \qquad \text{(B-38)}$$

$$\frac{\partial}{\partial i}F_{201} = \tfrac{3}{2}\sin i\cos i \qquad \text{(B-39)}$$

$$\frac{\partial}{\partial i}F_{202} = \frac{\partial}{\partial i}F_{200} \qquad \text{(B-39)}$$

$$\frac{\partial}{\partial i}F_{210} = \tfrac{3}{4}\left[2\cos^2 i + \cos i - 1\right] \qquad \text{(B-40)}$$

$$\frac{\partial}{\partial i}F_{211} = -\tfrac{3}{2}\left[2\cos^2 i - 1\right] \qquad \text{(B-41)}$$

$$\frac{\partial}{\partial i}F_{212} = -\tfrac{3}{4}\left[1 + \cos i - 2\cos^2 i\right] \qquad \text{(B-42)}$$

$$\frac{\partial}{\partial i}F_{220} = -\tfrac{3}{2}\sin i(1 + \cos i) \qquad \text{(B-43)}$$

$$\frac{\partial}{\partial i}F_{221} = 3\sin i\cos i \qquad \text{(B-44)}$$

$$\frac{\partial}{\partial i}F_{222} = \tfrac{3}{2}\sin i(1 - \cos i) \qquad \text{(B-45)}$$

References

[1]Carlisle, George, A. DiCicco, H. Harris, A. Salama, M. Vincent, *TOPEX/Poseidon Project Mission Plan*, Jet Propulsion Laboratory, JPL D-6862, rev. C, Aug. 1991 (Internal Document).

[2]Vincent, M. A., *TOPEX/POSEIDON Orbit Characteristics*, Jet Propulsion Laboratory, JPL D-7511, June 1990 (Internal Document).

[3]*TOPEX/POSEIDON Project Mission and Systems Requirements*, Jet Propulsion Laboratory JPL D-5901, April 1989 (Internal Document).

[4]Spier, Gerd W., *Design and Implementation of Models for the Double Precision Targeting Program (DPTRAJ)*, Jet Propulsion Laboratory, Technical Memorandum 33-451, April 15, 1971 (Internal Document).

[5]*DPTRAJ/ODP User's Reference Manual*, Jet Propulsion Laboratory, JPL D-263, Oct. 15, 1971 (Internal Document).

[6]*TOPEX Ground System Navigation Subsystem Software Requirements and Specifications Maneuver Analysis Software System*, Jet Propulsion Laboratory TOPEX/POSEIDON Project Document 633-743-21/22B (MASS SRD/SSD), JPL D-8740 (Internal Document).

[7]Cook, G. E., *Perturbations of Near-Circular Orbits by Earth's Gravitational Potential*, Royal Aircraft Establishment Technical Report #65252, Ministry of Aviation, Farnborough Hants, England, 1965.

[8]Guinn, J.R., "Short Period Gravitational Perturbations for Conversion Between Osculating and Mean Orbit Elements," AAS 91-430, *AAS/AIAA Astrodynamics Specialists Conference*, Durango, CO, August 19-22, 1991.

[9]Frauenholz, R. B., and Shapiro, B.E., "The Role of Predicted Solar Activity in TOPEX/POSEIDON Orbit Maintenance Maneuver Design," AAS 91-515, *AAS/AIAA Astrodynamics Specialists Conference*, Durango, CO, August 19-22, 1991.

[10]Bhat, R.S. , Frauenholz, R. B., and Cannell, P. E., "TOPEX/POSEIDON Orbit Maintenance Maneuver Design," AAS 89-408, *AAS/AIAA Astrodynamics Specialists Conference*, Stowe, VT, August 7-10, 1989.

[11]Bhat R. S., "TOPEX/POSEIDON Orbit Acquisition Maneuver Design," AAS 91-514, 1991 *AAS/AIAA Astrodynamics Specialist Conference*, Durango, Colorado, August 19-22, 1991.

[12]Escobal, Pedro Ramon, *Methods of Astrodynamics*, New York: Krieger, 1965.

[13]Merson, R.H., *The Dynamic Model of PROP, A Computer Program for the Refinement of the Orbital Parameters of an Earth Satellite*, Royal Aircraft Establishment, Technical Report #66255, Ministry of Aviation, Farnborough Hants, England, Aug. 1966.

[14]Groves, G. V. "Motion of a Satellite in the Earth's Gravitational Field," *Proc. Roy. Soc.* **254**, pp. 48-65, 1960.

[15]Kozai, Y., "The Motion of a Close Earth Satellite," *Astro. J.*, **64**, pp. 367-377, Nov. 1959.

[16]Vincent, M. A., "The Inclusion of Higher Degree and Order Gravity Terms in the Design of a Repeat Ground Track," AIAA-90-2899-CP, *AIAA/AAS Astrodynamics Conference*, Portland, Oregon, August 1990.

[17]Marsh, J. G., et. al., *The GEM-T2 Gravitational Model*, NASA Technical Memorandum 100746, Oct. 1989.

[18]Shapiro, Bruce, *TOPEX/POSEIDON Repeat Orbit and Reference Grid Definition*, Jet Propulsion Laboratory, IOM No. 314.5-1642, 22 June 1992 (Internal Document).

[19]Lerch, F. J., et. al., *Geopotential Models of the Earth from Satellite Tracking, Altimeter and Surface Gravity Measurements: GEM-T3, GEM-T3S*, NASA Technical Memorandum 104555, Jan. 1992.

[20]Kaula, William M., "Development of the Lunar and Solar Disturbing Function for a Close Satellite," *Astro. J.*, **67**:3, June 1962, pp. 300-303.

[21]Escobal, Pedro Ramon, *Methods of Orbit Determination*, New York: Krieger, 1983.

[22]Sterne, T.E., *An Introduction to Celestial Mechanics*, New York: Interscience, 1960.

[23]Roberts, C., "An Analytical Model for Upper Atmosphere Densities Based upon Jacchia's 1970 Models," *Celestial Mechanics*, **4**, pp. 368-377, 1971.